KSME

Springer

Journal of Mechanical Science and Technology 34 (5) 2020

Original Article
DOI 10.1007/s12206-020-0421-z

Keywords:
· Modified HP steel
· Creep modeling
· Secondary creep
· Tertiary creep
· Carbide precipitate
· G-phase
· Service aged

Correspondence to:
Kee Bong Yoon
kbyoon@cau.ac.kr

Citation:
Yu, J. M., Dao, V. H., Lok, V., Thi, G. L., Yoon, K. B. (2020). Asymptotic creep deformation behavior of modified HP steel after long-term service. Journal of Mechanical Science and Technology 34 (5) (2020) 1997~2009.
http://doi.org/10.1007/s12206-020-0421-z

Received October 21st, 2019
Revised February 19th, 2020
Accepted March 1st, 2020

† Recommended by Editor Chongdu Cho

Asymptotic creep deformation behavior of modified HP steel after long-term service

Jong Min Yu, Van Hung Dao, Vanno Lok, Thi Giang Le and Kee Bong Yoon

Department of Mechanical Engineering, Chung-Ang University, 84 Heukseok-ro, Dongjak-gu, Seoul 06974, Korea

Abstract Creep behavior of modified HP steel was investigated through the tensile creep tests under the stress conditions of 25-55 MPa at 950 °C with four reformer tubes of different service periods: Unused (virgin), 8.50, 9.67, and 16.17 year aged. The minimum creep strain rates, creep rupture life, as well as elongation and reduction of area of the ruptured specimen were measured. It was observed that all the measured properties did not vary with different service periods. The creep deformation behavior was modeled based on the experimentally measured creep data utilizing the secondary creep (SC) model, the tertiary creep (TC) model, and the combined model of two latter ones (SC-TC model). The results indicated the asymptotic creep deformation behavior of the secondary creep strain rate. The tertiary creep also demonstrated asymptotic behavior, however, its strain rate slightly increased, as the service period increased. The creep curves predicted by the SC-TC model were more accurate than those obtained using the SC or TC model. Microstructural observations supported the observed asymptotic behavior.

1. Introduction

Heater tubes which are the major components in process plants are filled with natural gas and steam together with catalysts. The tubes are heated in a furnace to obtain hydrogen-rich gas from hydro-cracking reaction at elevated temperature. The heater tubes are designed according to API 530 standard [1] to determine the wall thickness based on the allowable stress using the HK-40 alloy that implies limiting the tube diameter and thickness. Due to the fact that the size and thickness of the reformer tube are limited, its performance cannot be improved [2]. In recent years, after a new reformer design had been introduced, HP steel and the modified HP steel were mostly used to fabricate reformer tubes [2-4]. Owing to the improved creep resistance of the modified HP steel, the internal volume of the reformer tube was enhanced and reaction performance was increased by 30~40 %. Also the tube thickness was decreased, and therefore early creep damage could be prevented. It was known that the creep damage was accelerated by the large temperature gradient across the thick tube wall [2].

Centrifugally casted tubes made of the modified HP steel demonstrated excellent mechanical properties at high temperatures in the range of 900-1050 °C [3, 5]. The steel microstructure consisted of primary and secondary carbides (M_7C_3/MC and $M_{23}C_6$) precipitated at the grain boundary regions [6]. The precipitated carbides allowed preventing grain boundary sliding and restricting the motion of dislocations [7]. It was reported that the resistance against the high temperature creep was obtained by increasing the Cr, Ni composition, or by micro-alloying with 1 % Nb along with performing stabilized fine dispersion of NbC carbide particles [5, 8, 9]. However, long-term service life of the modified HP steel was not well investigated. It was considered that it had to be closely related to the environment conditions such as the high temperature and applied stress. Often, the actual service life of the modified HP steel was shorter than the designed creep life of 100000 h. In many cases, reported premature failures were mainly attributed to the creep deformation, microstructural degradation, and formation of creep voids [10-14]. Therefore, it is an important challenge to understand the creep behavior during various

service periods of the modified HP steel used for the reformer tubes.

Recently, several studies investigated the secondary creep deformation behavior of the HP grade material [7, 12, 15-17]. They attempted to explain the reasons for different results of creep tests modeled based on the Norton's power-law and Sherby-Dorn equation under various conditions of a test temperature or a service period. The tertiary creep mechanism was also studied, as the tertiary creep damage appearing in the last stage of creep was important [3]. Creep damage in the tertiary creep stage of the HP grade steel was quantified by applying the continuum damage mechanics model. Coupling between creep deformation and creep damage in the tertiary stage was also investigated using nickel-based superalloys [18-20].

In this study, the creep behavior of the modified HP steel was investigated at 950 °C with tube specimens of four different service periods. The creep deformation behavior was modeled based on the experimental data using the secondary creep model, the tertiary creep model, and the combined one of these two. The results indicated the presence of the asymptotic creep deformation behavior of the secondary creep strain rate in the case when the service period of the steel was longer than 8.50 years. The tertiary creep also showed asymptotic behavior, however, the tertiary creep strain rate was slightly increased as the service period increased. Microstructural observations supported the observed behavior.

2. Experimental procedures

2.1 Reformer tubes and specimens of different service periods

Reformer tubes manufactured through centrifugal casting of the austenitic modified HP steel are installed vertically in a reforming furnace as depicted in Fig. 1. Reformer tube system was designed to expand freely in vertical direction. There was no axial constraint generating thermal stress during start-up and shut-down operation. The chemical composition of the modified HP ASTM A608 steel is provided in Table 1. The full tube length was 14 m; the internal diameter was 122.6 mm; and the wall thickness was 12 mm. Operating condition of the tubes was 950 °C under the maximum internal pressure of 33 bars with the design service life of 100000 h (11.4 years) [2, 4, 6]. The feed gas and steam entered from the top of the tube and flowed down through the catalyst filled in the tubes as shown in Fig. 1.

A domestic reforming furnace was shut down for a planned overhaul. Four reformer tubes with different service periods were selected and taken out for analysis. A tube segment of 0.4 m length was cut out from the heated zone portion located about 7 m above from the bottom of the furnace where no weld joint was included. Another tube segment was also taken from the tube outside of the furnace bottom where the temperature was low. This section of the tube did not experience any contact of internal hot fluid and external hot flue gas. This part of

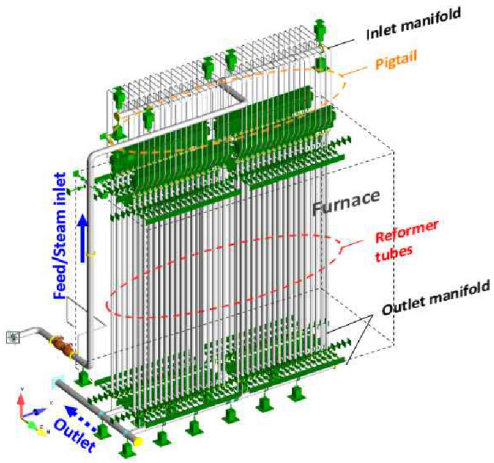

Fig. 1. Reforming heater structure and reformer tubes.

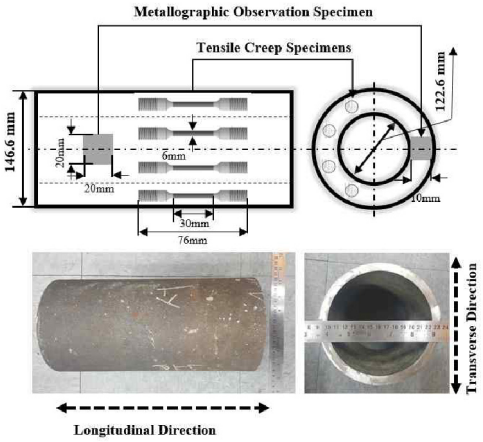

Fig. 2. Schematic illustration of the specimens sampling location for a rectangular block and tensile creep testing specimens from each of the modified HP reformer tube.

the tube can be considered as an unused (virgin) material, which was not aged during the service period. The service periods of the other considered tubes were 8.50, 9.67, and 16.17 years. Detailed information on the reformer tubes is presented in Table 2 and Fig. 2. As shown in Fig. 2, block specimens with dimension of 20×20×10 mm and tensile creep test specimens with the diameter of 6 mm and the gauge length of 30 mm were machined in axial direction.

2.2 Tensile creep test

Tensile creep tests were conducted at 950 °C under the stress range of 25-55 MPa in accordance with the ASTM E139 standard [21]. The testing conditions are summarized in Table 3 for 16 creep tests conducted. The creep curve was recorded by logging the data on creep strain versus time using a data acquisition computer. The creep strain versus time data were converted to the creep strain rate versus elapsed time ones using the seven-point incremental polynomial method specified in the ASTM E647 standard [22]. The minimum creep strain

Table 1. Chemical composition of the modified HP steel according to ASTM A608 (wt%).

Material	C	Ni	Cr	Nb	Si	Mn	Mo	Fe
Modified HP steel	0.38-0.45	34-37	24-27	0.5-1.5	0.5-1.5	≤ 1.5	0.50	Bal

Table 2. Service histories of four differently aged reformer tubes.

Tube No.	#4	#53	#52	#26
Installation	-	2005.07	2005.07	1997.10
Taken-out	-	2013.12	2015.03	2013.12
Serviced period (years)	0 (virgin)	8.50	9.67	16.17

rate was estimated from the data in the given time range corresponding the lowest creep strain rate for each case. In addition, the reduction of area and the percent elongation were determined from the ruptured section of the creep specimens following ASTM E139 standard (Secs. 8.8.1 and 8.8.2). The obtained results of rupture time, reduction of area, percent elongation and minimum creep strain rate are summarized in Table 3.

2.3 Microstructural observation

To investigate the microstructural degradation and carbide transformations after long-term service, scanning electron microscopy (SEM), and energy-dispersive X-ray spectroscopy (EDS) were applied. Besides of high magnification of the regular SEM observation, backscattered electron (BSE) images were obtained to identify different kinds of carbides. EDS element mapping was also used to analyze the distributions of a Nb, Si, and Cr.

Block specimens machined from the reformer tubes as shown in Fig. 2 were prepared for metallography. The specimens were grounded with water using silicon carbide papers with the grit size of 320-2400 and polished on a cloth using 0.6-0.1 μm diamond suspensions. Ultrasonic cleaning was used for 5 minutes in the ethanol solution. Etching was finally conducted for the solution of HNO_3, HCl, and glycerol, before observing the specimens with SEM.

3. Results and discussion

3.1 Creep tests

3.1.1 Creep deformation and creep rupture life

Fig. 3 shows the creep strain versus elapsed time curves obtained as a result of the conducted creep tests. For each aged condition, four creep curves were measured under different stress levels. From the creep curves presented in Figs. 3(a)-(d), the creep strain rate versus time curves were generated and plotted as shown in Figs. 4(a)-(d). The elapsed time was normalized by the rupture time t_r and expressed as t/t_r. By normalizing the time axis, the primary, secondary, and tertiary creep stages could be easily identified and compared with each other for all tested specimens.

In the creep curves corresponding to the virgin material of the modified HP steel shown in Figs. 3(a) and 4(a), the secondary creep stage was more prevalent comparing with the cases of the aged materials. However, the tertiary creep stage became dominant in all other three cases corresponding to the service period of 8.50, 9.67, and 16.17 years, particularly, when the lower stress was applied as shown in Figs. 4(b)-(d). It should be noted that the primary creep stage at the early time after loading was neglected and taken out of consideration in present study. The tertiary creep started at 27-48 % of the creep life, except for two other cases, when the virgin material tests were conducted under 40 and 45 MPa applied stresses. In these cases, the tertiary creep stages were observed after 61 % and 81 % of the creep life. In Fig. 4, the secondary creep strain rate values are presented as solid lines parallel to the X-axis. When the strain rate was increased noticeably with respect to the secondary creep strain rate, it was assumed that the tertiary creep started. The starting time of the tertiary creep was estimated and presented in the graph along with the corresponding t/t_r values. For the virgin material, t/t_r values of 0.28, 0.37, 0.61 and 0.81 were shown in Fig. 4(a); and for the 16.17 year aged material, t/t_r values of 0.27, 0.30, 0.40 and 0.44 were shown in Fig. 4(d).

The reduction of area measured at the necked region of the creep ruptured specimens was 15.98 % for the virgin material. Subsequently, it was increased by 39.40, 39.21 and 35.52 % for the tube materials with service periods of 8.50, 9.67, and 16.17 years, respectively. The percent elongation was also measured. The percent elongation of the virgin material was 19.33 %. For the aged materials, it was 30.84, 40.00, and 35.42 % for the service periods of 8.50, 9.67, and 16.17 years, respectively. For all three considered service periods, we did not observe the considerable difference in the reduction of area and the percent elongation results, however, they were significantly higher than those of the virgin material.

Numeric data for all individual creep tests, such as the creep rupture life, minimum creep strain rate, reduction of area, and percent elongation, are summarized in Table 3. As expected, the virgin material demonstrated longer creep life than the aged materials under the same applied stress [12, 23]. Under the applied stress of 40 MPa, the creep life of the virgin material was 219.87 *h*, and those of the aged material was 34.27 *h*, 35.82 *h*, 34.42 *h* for the service periods of 8.50, 9.67, and 16.17 years, respectively. Considering the tests under the applied stress of 40 MPa, the minimum creep strain rate of 1.70×10^{-4} h^{-1} was obtained for the virgin material; and the creep strain rates of 4.90×10^{-3} h^{-1}, 5.30×10^{-3} h^{-1}, and 5.10×10^{-3} h^{-1} was obtained for the service period of 8.50, 9.67, and 16.17 years, respectively, indicating the lower creep deformation resistance of the aged materials. Even though the service period varied from 8.50 to 16.17 years, material creep properties did not change considerably but appeared to approach nearly constant values. The creep properties approach asymptotic

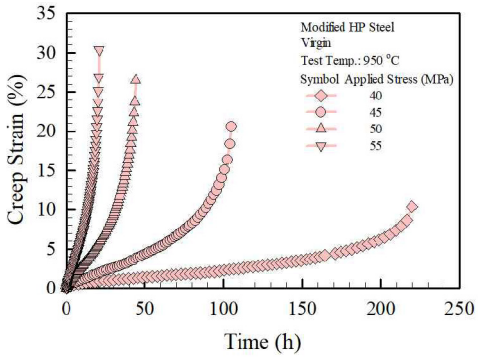

(a)

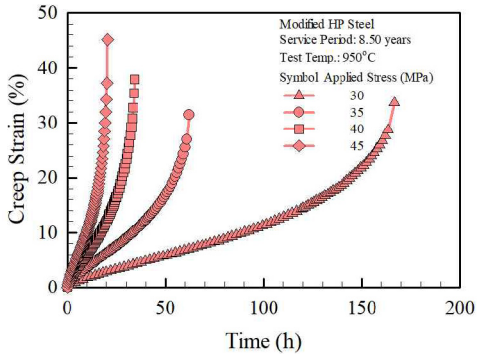

(b)

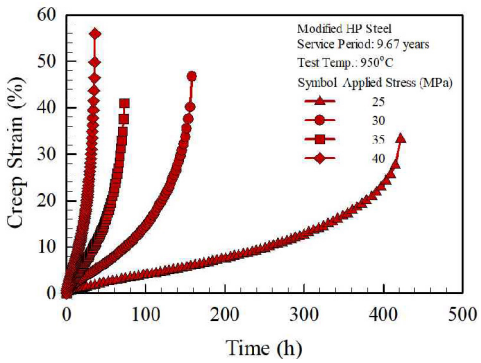

(c)

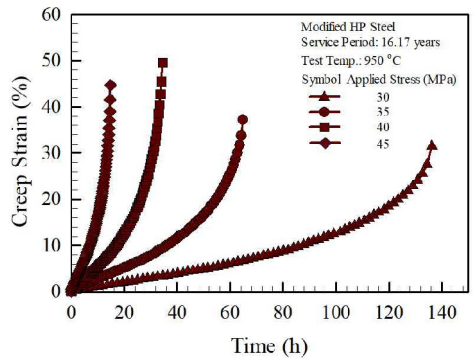

(d)

Fig. 3. Creep curves showing creep strain versus testing time for the modified HP steel at 950 °C: (a) Virgin material; (b) 8.50 year serviced; (c) 9.67 year serviced; (d) 16.17 year serviced material.

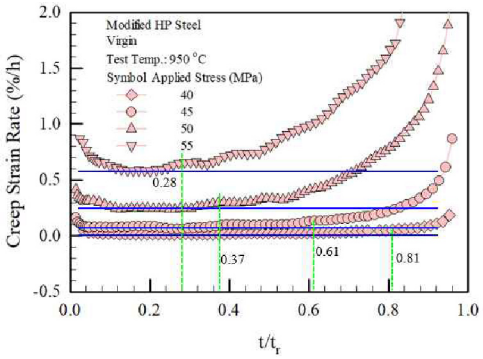

(a)

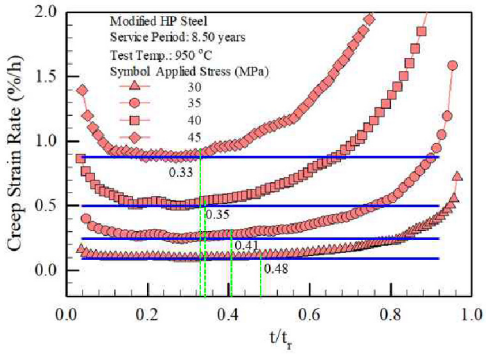

(b)

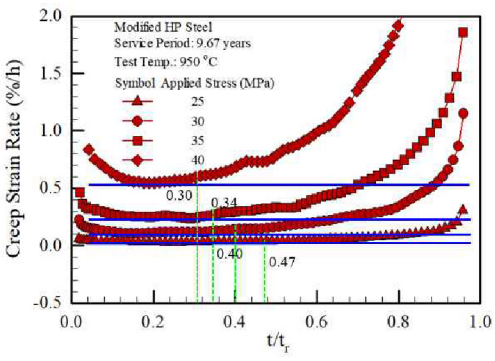

(c)

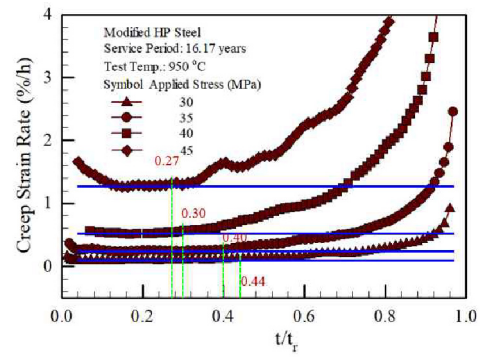

(d)

Fig. 4. Creep strain versus time fraction (t/t_r) curves for the modified HP steel at 950 °C for determining the minimum creep strain rate and the time for starting the tertiary creep: (a) Virgin material; (b) 8.50 year serviced; (c) 9.67 year serviced; (d) 16.17 year serviced material.

Table 3. Creep test results of four differently service aged modified HP steels at 950 °C.

Tube No.	Service aged period (year)	Applied stress (MPa)	Time to rupture (h)	Reduction of area (%)		Elongation (%)		Min. creep strain rate (h^{-1})
				Specimen	Avg.	Specimen	Avg.	
#4	0 (virgin)	40	219.87	8.67	15.98	7.33	19.33	1.70E-04
		45	104.82	14.58		16.67		5.50E-04
		50	44.10	17.83		25.00		2.45E-03
		55	20.87	22.87		28.33		5.85E-03
#53	8.50	30	166.55	32.25	39.40	26.67	30.84	9.45E-04
		35	62.07	41.25		21.67		2.45E-03
		40	34.27	37.89		33.33		4.90E-03
		45	20.53	46.22		41.67		8.50E-03
#52	9.67	25	421.53	37.17	39.21	28.33	40.00	2.95E-04
		30	158.48	37.25		41.67		9.50E-04
		35	72.97	39.17		40.00		2.00E-03
		40	35.82	43.25		50.00		5.30E-03
#26	16.17	30	136.23	32.92	35.52	26.67	35.42	8.80E-04
		35	64.82	37.83		31.67		1.85E-03
		40	34.42	28.42		43.33		5.10E-03
		45	14.77	42.92		40.00		1.22E-02

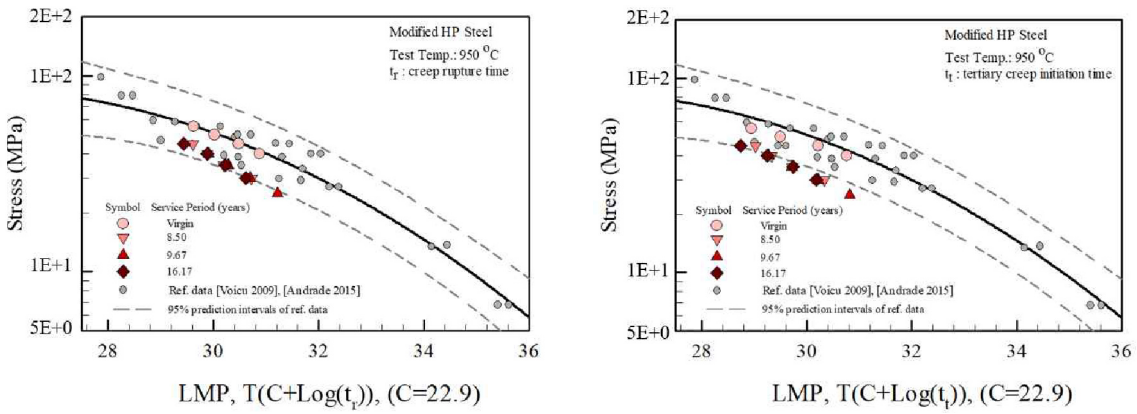

Fig. 5. Larson-Miller diagram with C = 22.9 for the modified HP steel using t_r (a) as the creep rupture failure time; (b) as the tertiary creep initiation time indicating creep cavitation.

values representing the full aging condition of the materials.

The Larson-Miller parameter (LMP) curve widely used to determine the remaining life or the balanced rupture life of aged reformer tubes is analyzed in this study. The measured creep rupture lives for the virgin and the service-exposed modified HP steels are presented in Fig. 5(a). The Larson-Miller parameter (LMP) values were determined as $P = (T+273)\times(22.9+Log t_r)$ where, P is the LMP parameter, t_r is the stress rupture time, T is the temperature (in Kelvin), and C = 22.9 is the Larson-Miller constant. The experimental data were plotted and then, compared to those reported in the Refs. [15, 24]. Most of the data obtained for the virgin HP steel specimens were located on the 95 % prediction line. In turn, the data obtained using the reformer tubes with the service periods of 8.50, 9.67, and 16.17 years, are below the scatter band corresponding to the virgin and manufacturer creep curves. Significant reduction in the creep rupture life for the case of aging tubes is observed.

In determining the LMP values, the time, t_t, marked when the tertiary creep stage started, was used instead of the creep rupture time, t_r. The LMP values were determined by $P = (T+273)\times(22.9+Log\ t_t)$. The obtained results are presented in Fig. 5(b). The observed curve shows a similar tendency with Fig. 5(a), however, it demonstrates better correlation with the LMP curves. In the actual industry practice, the tube service life is considered to be finished, when creep cavities are detected by field replication method during a turn-around inspection. Therefore, the creep life can be defined as the initiation of the

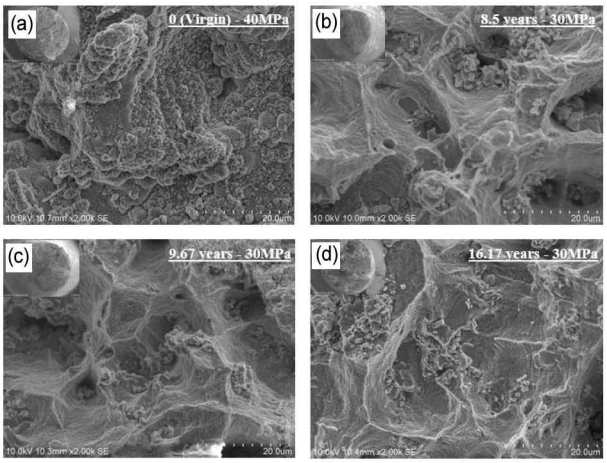

Fig. 6. SEM image (×30 vs. ×2000 magnification) fracture surface on ruptured specimens: (a) Virgin-40 MPa; (b) 8.50 years-30 MPa; (c) 9.67 years-30 MPa; (d) 16.17 years-30 MPa.

tertiary creep to maintain more safe operation and to assess the residual life of the reformer tubes conservatively.

The fracture surfaces of the creep ruptured specimens under the similar stress level of 30-40 MPa were observed for the virgin and service-exposed specimens, as shown in Fig. 6. The fracture surface appearance was rather similar for the tube materials with service periods of 8.50, 9.67, and 16.17 years. The fracture surfaces demonstrated the ductile fracture and consisted of several dimples and precipitates, as shown in Figs. 6(b)-(d). However, for virgin material the surface fracture appearance showed more brittle features that the aged ones as shown in Fig. 6(a). The aged specimens showed more intergranular fracture appearances comparing to the virgin specimen. Intergranular fracture of the aged materials indicates that the fracture originates at the grain boundary [5]. Moreover, it implies that the cavity formation, growth and linkage indicated a transition from the intergranular-transgranular combined fracture to the fully intergranular fracture. It should be taken into account that the grain boundary strength of the virgin material is higher than those of the service-exposed materials. The intergranular creep failure is more probable, if the modified HP steel is aged during the service, and the grain boundary became weaker comparing with the virgin steel.

3.2 Modeling of creep for the modified HP steel

The creep curves measured for the modified HP steel as shown in Fig. 3, had negligible primary creep contribution. Therefore, while modeling the creep strain generated by the applied stress, we considered only the creep strain contributions due to the secondary creep (SC) and the tertiary creep (TC). Three different creep deformation models were employed in this study: the secondary creep (SC) model, tertiary creep (TC) model, and secondary creep-tertiary creep (SC-TC) combined model. Implementation of each model was performed

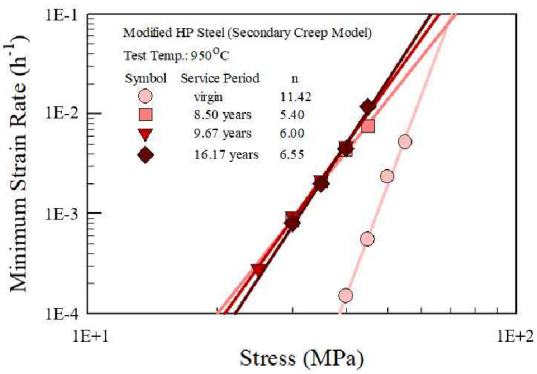

Fig. 7. Determination of the constants for the secondary creep (SC) model from linear regression lines between the applied stress and the minimum creep strain rate.

based on the measured creep data. The analysis results are presented in the subsections below as follows.

3.2.1 Secondary creep (SC) model

In the related studies, the SC model was applied to most of the heat resistance steels with a creep curve having the dominant secondary creep stage. In this model, total strain is assumed to be equal to the secondary creep strain. The relationship between the secondary creep strain rate, which is the minimum creep strain rate, and the applied stress is expressed using the Norton's power law as shown in Eq. (1).

$$\dot{\varepsilon} = \dot{\varepsilon}_{SC} = A\sigma^n \tag{1}$$

Here, $\dot{\varepsilon}_{SC}$ is the time rate of secondary creep strain, σ is the applied stress and *A* and *n* are the secondary creep coefficient and the secondary creep exponent, respectively [12]. The minimum secondary creep strain rates measured for all sixteen specimens are summarized in Table 3, and represented in Fig. 7 as a function of the applied stress. As the log-log scale is used, the slope of linear regression line provides the creep exponent value for the virgin and the aged steels.

The linear regression results are shown in Fig. 7, and the obtained secondary creep constants, *A* and *n* are provided in Table 4. The secondary creep exponent was 11.42, 5.40, 6.00, and 6.55, for the service periods of 0.00 (virgin), 8.50, 9.67, and 16.17 years, respectively. The creep exponent decreased considerably from 11.42 to 5.40 after the service period of 8.50 years. However, the exponent value did not change significantly, when the service period extended to 16.17 years, levelling off to almost constant value. Therefore, the regression lines of three differently aged steel between 8.5 and 16.17 years overlapped, as shown in Fig. 7. The regression line corresponding to the virgin steel locates much lower indicating that the creep deformation resistance of the virgin material is much higher than those of the aged materials. Therefore, it can be considered that the secondary creep deformation behavior, which is represented by the minimum creep strain rate, showed an asymptotic behavior, when the service period was longer

Table 4. Creep deformation constants for the modified HP steel at 950 °C based on the secondary creep (SC) model.

Reformer tube No.	Service period (year)	Secondary creep constants	
		A [$h^{-1}MPa^{-n}$]	n
#4	0 (virgin)	7.71E-23	11.42
#53	8.50	9.18E-12	5.40
#52	9.67	1.19E-12	6.00
#26	16.17	1.58E-13	6.55

Table 5. Creep deformation constants for the modified HP steel at 950 °C based on the tertiary creep (TC) model.

Reformer tube No.	Service period (year)	Tertiary creep constants		
		A_3 [$h^{-1}MPa^{-n_3}$]	n_3	p_3
#4	0 (virgin)	1.74E-19	10.0	0.48
#53	8.50	7.02E-11	5.35	0.51
#52	9.67	2.90E-11	5.64	0.52
#26	16.17	2.76E-11	5.72	0.56

than 8.50 years for the service-exposed modified HP steel. The modified HP steel needs to be controlled by the dislocation creep mechanism, as the creep exponent value is in the range of 3-12 [16, 25].

The SC model provides the constant creep strain rate value, when the applied stress is constant. Significant error exists between the strain rate predicted by the SC model and the actual measured strain rate, as shown in Fig. 4. This error became larger as the elapse time t/t_r increased, particularly, when t/t_r was over 0.5. For the modified HP steel, the tertiary creep has to be introduced while modeling the creep deformation.

3.2.2 Tertiary creep (TC) model

In the tertiary creep (TC) model, the total creep strain was considered to be equal to the tertiary creep strain. The secondary creep was not included in estimating the creep strain. The constitutive equation for the TC model is shown in Eq. (2):

$$\dot{\varepsilon} = \dot{\varepsilon}_{TC} = A_3 \sigma^{n_3} \varepsilon^{p_3} \tag{2}$$

where $\dot{\varepsilon}_{TC}$ is the time rate of the tertiary creep strain, ε is the total creep strain and A_3, n_3, and p_3 are the tertiary creep constants. As only the tertiary creep strain was considered in this model excluding the secondary one, the tertiary creep strain, ε_{TC}, was actually equal to the total creep strain, ε. For each considered service period, the tertiary creep constants of the TC model were determined from the experimental data by regression. The obtained results are shown in Table 5. The same number of data points for each creep test condition was used in regression so that the weight of each test could be the same in terms of determining the model constants.

In Fig. 8, the stress dependent term of the creep strain rate, $\dot{\varepsilon}_{TC} / \varepsilon_{TC}^{p_3}$, was used in Y-axis. Then, this can be a function of the applied stress only. Sixteen creep test datasets and the corresponding regression lines are shown in Fig. 8.

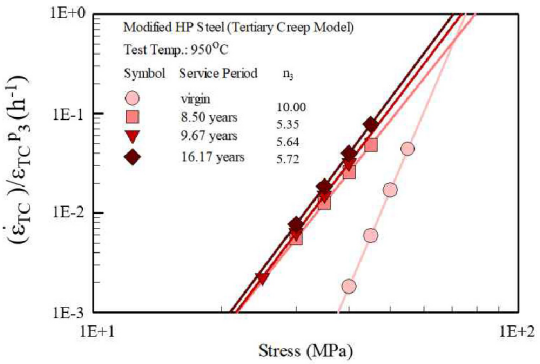

Fig. 8. Determination of the creep exponents for the tertiary creep (TC) model from the relationship between the applied stress and the stress dependent term of the creep strain rate, $\dot{\varepsilon}_{TC} / \varepsilon_{TC}^{p_3}$.

Thereafter, similar to the SC model, the tertiary creep exponent was 10.00, 5.35, 5.64, and 5.72, for the virgin, 8.50, 9.67 and 16.17 year aged material. The tertiary creep exponent decreased considerably from 10.00 to 5.35 after the service period of 8.50 years. However, the exponent value changed only slightly from 5.35 to 5.72 even when the service period increased from 8.50 years to 16.17 years. Similarly, in the TC model, an asymptotic behavior of creep properties was confirmed for the service-exposed modified HP steel.

The accuracy of the TC model was analyzed in Fig. 9 that shows the comparison between the measured creep stain and the predicted creep strain using Eq. (3) of the TC model. Eq. (3) was obtained by integrating Eq. (2) with respect to time:

$$\varepsilon = \varepsilon_{TC} = \left[A_3 (1 - p_3) \sigma^{n_3} t \right]^{\frac{1}{1-p_3}} \tag{3}$$

The TC model creep strain values were plotted using different kind of lines, and the experimental data were plotted using symbols. As shown in Fig. 9, the accuracy was improved in the later part of the creep curves. However, at the early part of the creep curves the TC model could not predict the actual creep behavior reasonably. Therefore, to facilitate a better prediction model for the creep strain of the modified HP steel, the secondary creep, and the tertiary creep need to be combined together.

3.2.3 Secondary creep-tertiary creep (SC-TC) model

To account for the creep deformation behavior in the secondary creep stage, as well as the creep cavitation damage accumulation in the tertiary creep stage of the modified HP steel, the SC model and the TC model needed to be combined together. In this combined model, the total creep strain was assumed as a summation of the secondary creep and the tertiary creep was defined as shown in Eq. (4) [26].

$$\begin{aligned} \dot{\varepsilon} &= \dot{\varepsilon}_{SC} + \dot{\varepsilon}_{TC} \\ &= A\sigma^n + A_3 \sigma^{n_3} \varepsilon_{TC}^{p_3} = A\sigma^n + A_3 \sigma^{n_3} (\varepsilon - A\sigma^n t)^{p_3} \end{aligned} \tag{4}$$

Table 6. Creep deformation constants for the modified HP steel at 950 °C based on the secondary creep-tertiary creep (SC-TC) model.

Tube No.	Service period (year)	Secondary creep - tertiary creep constants				
		A [$h^{-1}MPa^{-n}$]	n	A_3 [$h^{-1}MPa^{-n_3}$]	n_3	p_3
#4	0 (virgin)	7.71E-23	11.42	9.78E-18	9.55	1.16
#53	8.50	5.42E-13	6.15	5.26E-10	5.24	1.13
#52	9.67	6.87E-13	6.15	9.44E-10	5.11	1.13
#26	16.17	7.72E-13	6.15	3.47E-10	5.45	1.02

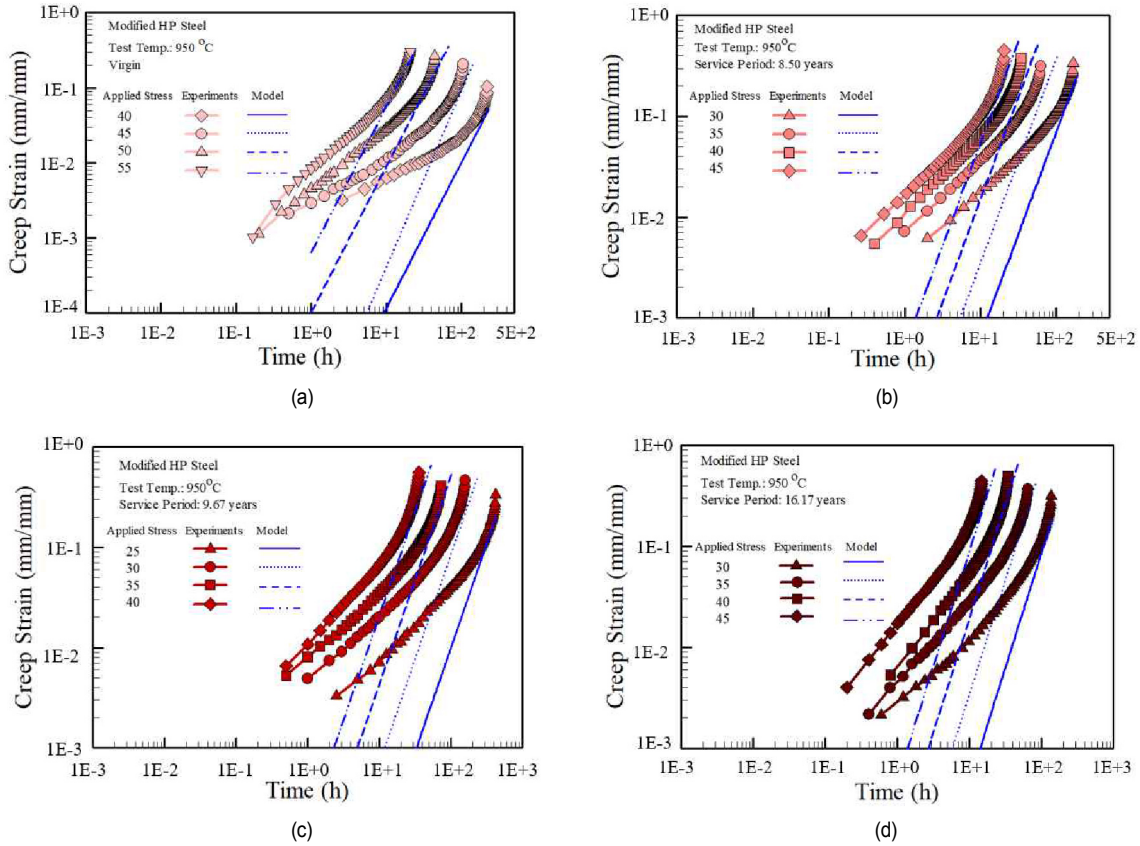

Fig. 9. Comparison between experimentally measured creep data and simulation data based on the tertiary creep (TC) model: (a) Virgin material; (b) 8.50 year serviced; (c) 9.67 year serviced; (d) 16.17 year serviced material.

In the SC-TC model, the Norton's power law creep model was used as the secondary creep strain rate contribution which provides a constant value if the applied stress is constant. The tertiary creep model was expressed as a tertiary creep strain rate which provides higher values as the tertiary creep strain is accumulated. It should be noted that the tertiary creep depends on the accumulated tertiary creep strain, not on the accumulated total strain. In Eq. (4), the tertiary creep strain, $\varepsilon - A\sigma^n t$, in which the accumulated secondary creep strain value was removed from the total creep strain value, was used instead of the total creep strain value.

In the SC-TC model, five creep constants, *A, n, A_3, n_3,* and *p_3*, needed to be determined. For the secondary creep strain prediction, the constants *A* and *n* obtained as shown in Fig. 7, could be used. However, the predicted secondary creep strain rates outside of the stress range (25~45 MPa) of the creep testing provided significant scatter, whose level was different for each service period. To reduce this scatter, a mean value for the secondary creep exponent, *n*, was used for three considered service periods in the SC-TC model. Prediction error of the creep strain caused by the contribution of the secondary creep could be minimized by using the mean value of *n*. The tertiary creep constants *A_3, n_3,* and *p_3* were determined by regression. The obtained constants *A, n, A_3, n_3,* and *p_3* are presented in Table 6. The average *n* value across the service period of 8.50, 9.67, and 16.17 was 6.15.

In the SC-TC model, the tertiary creep strain rate term excluding the secondary creep one from the total strain rate, $(\dot{\varepsilon} - A\sigma^n) / (\varepsilon - A\sigma^n t)^{p_3}$, is shown in the Y-axis in Fig. 10. For the virgin materials it was lower than the other three aged materials. All three aged materials showed similar tertiary creep strain rate values. As the service period was increased from

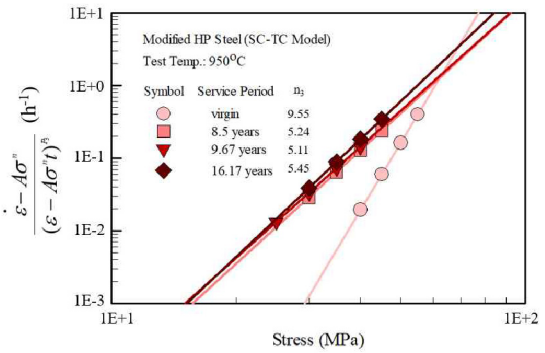

Fig. 10. Determination of the tertiary creep exponent, n_3, for the secondary creep-tertiary creep (SC-TC) model from the relationship between the applied stress and the stress dependent term of the tertiary creep strain rate, $(\dot{\varepsilon}-A\sigma^n)/(\varepsilon-A\sigma^n t)^{n_3}$.

8.5 years to 16.17 years the tertiary creep strain rate was increased slightly but its difference was not significant. The same asymptotic behavior similar to what was shown in Figs. 7 and 8, was verified in the SC-TC model.

Figs. 11(a)-(d) represent the comparison between the measured and predicted creep strain data in the SC-TC model using the creep constants (A, n, A_3, n_3, and p_3) in Table 6 and Eq. (4). To ensure clear comparison, the log-log scale was used for creep curves. As shown in this figure, the predicted creep curves obtained using the SC-TC model were significantly more accurate than those of the cases using the SC model or the TC model only. Therefore, we conclude that for service aged reformer tubes made of the modified HP steel, the SC-TC creep model can be applied efficiently for predicting the accumulated creep deformation such as tube expansion or creep damage.

3.3 Observations on the microstructures supporting the asymptotic creep behavior

Fig. 12 shows the microstructures of the modified HP steel corresponding to the virgin specimen under high magnifications (×1000). In Fig. 12(a) that represents grain boundary regions of the virgin steel, it can be seen that continuous networks of primary carbides appeared as an inter-dendritic pattern formed during solidification of the reformer tube. Two types of the second-phase particles at the grain boundaries were indicated by the arrows in Fig. 12(a), i.e., Nb-rich carbides and Cr-rich carbides. The backscattered electron (BSE) image and EDS analysis results for these carbides are shown in Fig. 12(a). It was observed that the white precipitates composed mainly of Nb (68.88 wt.%) were considerably fine. Niobium was combined with carbon to form MC, in which M was a metal element, most of which corresponded to Nb element [5, 27]. NbC was stable at the high temperature [15]. The lattice stability of the MC precipitates is known to be caused by the Gibbs energy of the compound, which depends on the composition at a given temperature [28]. Therefore, increasing the number of MC precipitates could improve the creep rupture time and reduce

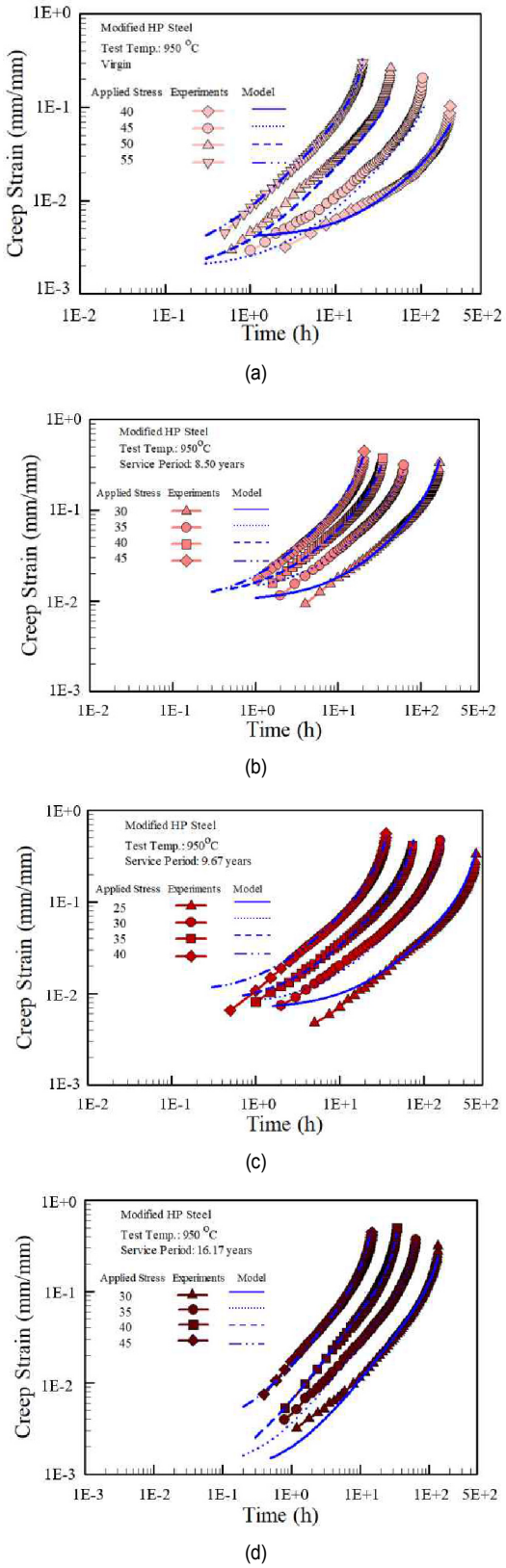

Fig. 11. Comparison between experimentally measured creep data and simulation data based on the secondary creep-tertiary creep (SC-TC) model: (a) Virgin material; (b) 8.50 year serviced; (c) 9.67 year serviced; (d) 16.17 year serviced material.

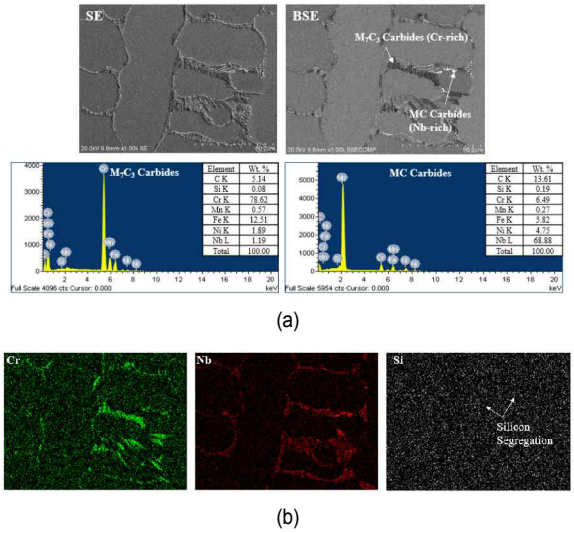

Fig. 12. Microstructure of modified HP steel before the creep test of virgin material: (a) Scanning electron microscope (SEM), backscattered electron (BSE) images, and EDS analysis result of an MC and M_7C_3 precipitates; (b) EDS element maps for Cr, Nb and Si.

minimum creep strain rates [5, 7]. However, precipitates in black contrast were identified as Cr-rich M_7C_3 carbides, in which most of M metal corresponded to Cr elements (78.62 wt.%). The Cr-rich carbides have deleterious effects on the creep resistance of the modified HP steel, when they become coarsening, as reported in previous studies [4, 6, 10]. Fig. 12(b) represented the EDS element maps of Cr, Nb, and Si, which served to identify where MC and M_7C_3 carbides were located. Si segregation was observed at the austenite inter-dendritic boundaries during solidification followed by the primary carbide formation. There was no strong concentration of Si overlapping with the Nb-rich regions. This observation indicated that the white areas in the Nb map corresponded to MC carbide, not G-phase.

The microstructures of the aged specimens with the service period of 8.50, 9.67, and 16.17 years are shown in Fig. 13. The microstructure exhibited coarsened inter-dendritic carbides, the network continuity of $M_{23}C_6$ and bright G-phase (see Figs. 13(a)-(c)), which were defined as secondary carbides. In comparison to the virgin specimen, carbides were linked with neighboring ones along the grain boundaries and became coarsened making blocky and spheroidal shapes. Transformation of the primary carbides into the secondary carbides was observed in the BSE images and confirmed by the EDS analysis results, as shown in Figs. 13(d)-(h). The $M_{23}C_6$ precipitates were observed along the grain boundaries in the serviced materials, and the lattice parameter of $M_{23}C_6$ increased and became more visible as the service aged period increased [29]. The granular shape changed gradually from the fine shape to coarse one, as shown in Figs. 13(d)-(f). Reduction of the creep life of the aged steels was attributed to the increase in the size of $M_{23}C_6$ precipitates [12]. Moreover, these coarsened precipitates are more prone to form cavities and micro-cracks than

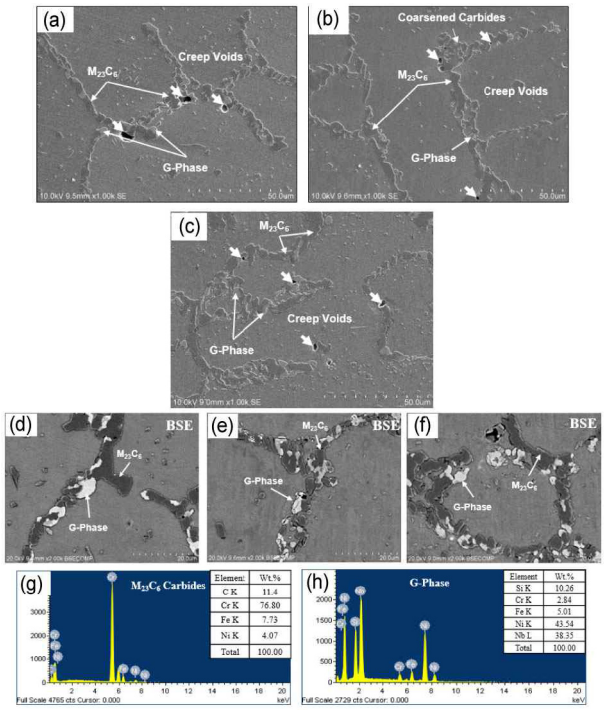

Fig. 13. SEM images of the modified HP steel before the creep test service aged for (a) 8.50 years; (b) 9.67 years; (c) 16.17 years. Backscattered electron (BSE) images and EDS analysis of the specimen aged for (d) 8.50 years; (e) 9.67 years; (f) 16.17 years with EDS analysis results of (g) $M_{23}C_6$ precipitate; (h) G-phase.

other precipitates [10]. Significant amount of silicon and nickel elements appeared in the white areas in the aged materials with the service period of 8.50, 9.67, and 16.17 years, confirming that the MC precipitates were not stable, and tended to transform into the G-phase which mainly consisted of niobium (38.35 wt.%), silicon (10.26 wt.%), and nickel (43.54 wt.%) as shown in Fig. 13(h). Consequently, volumetric fraction of precipitated carbides of the serviced materials were larger than that of the virgin material, as shown in Figs. 13(d)-(f). Similar to other precipitates, the G-phase increased as the service period increased, and this also resulted in negative effects to the creep resisting properties. The G-phase also provided the preferential site for creep damage [4, 13]. Fig. 14 showed the results of the EDS element Nb, Si, Ni, and Cr map from BSE image represented in Fig. 13(d). It showed coarsened inter-dendritic carbides that were supposed to be transformed from primary M_7C_3, and MC carbides to secondary $M_{23}C_6$ carbide and G-phase, respectively. It should be noted that G-phase corresponded to the majority of the bright spots, which replaced MC of the major precipitates. It was formed by consuming silicon (Si) segregated at the inter-dendritic boundaries. High concentration of silicon in the bright phase location was observed, where the niobium and nickel concentrations were also high, as shown in Fig. 14. Therefore, silicon was deemed to be the main factor to control G-phase formation among the constituent elements.

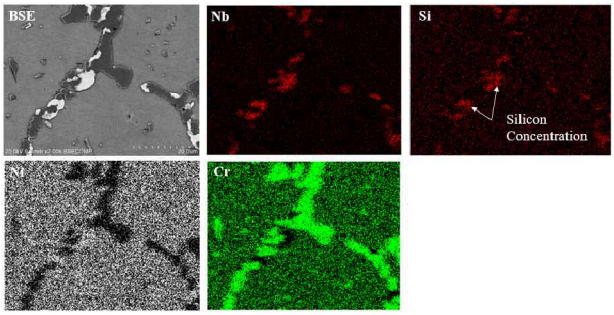

Fig. 14. Backscattered electron (BSE) image and EDS element distribution maps for Nb, Si, Ni and Cr with the modified HP steel service aged for 8.5 years.

The initial microstructure was noticeably changed, and after 8.50 years of service it reached almost unchanged condition showing the coalescence and coarsening of carbides until 16.17 years of service. The minimum secondary creep strain rate values measured for all aged specimens were almost similar under the same stress level as the aging time was increased from the 8.50 years to 16.17 years, as outlined in Table 4. Therefore, the secondary creep deformation represented by the minimum creep strain rate indicated the asymptotic behavior of the service-exposed modified HP steel, as presented in Fig. 7.

It was shown that the coarsening of the secondary carbides such as $M_{23}C_6$ and G-phase precipitates was due to the microstructural changes from the initial primary carbides. Formation of the secondary carbides was supposed to be proportional to the service period [4, 29]. Creep voids formation near the secondary carbides can be verified in Figs. 13(a)-(c), which indicate that the creep damage is accumulated, as the service time became longer. Generally, the tertiary creep stage appears due to connection and growth of creep voids, and these grain boundary cavities acting as efficient vacancy sinks lead to acceleration of creep resulting in a high strain rate [30]. Therefore, in the TC model and the SC-TC model, it appeared that the tertiary creep strain rate was increased, as the service period of the modified HP steel became longer, as shown in Figs. 8 and 10. However, the extent of increase was insignificant. It explained the observed fact that the number of creep voids increased quickly in the tertiary creep region [3], which was shown in the creep curves of the aged specimens, as the earliest starting time and the longest tertiary stage.

4. Conclusions

In this study, tensile creep tests were conducted at 950 °C using long-term service aged reformer tube specimens to investigate the creep deformation and rupture behavior and its relevance to microstructural change of the modified HP steel. In the experiments, we considered different service periods of the test tubes: Unused; 8.50; 9.67; and 16.17 years. The following conclusions were derived:

(1) When the service period varied from 8.50 to 16.17 years, material creep properties such as the creep rupture life and elongation at failure, and the minimum creep rates did not change significantly, however, they appeared to approach nearly constant values. Nevertheless, it was considered that most of the creep properties approached asymptotic values representing the full aging condition of the materials.

(2) The measured creep curves were represented by three different creep deformation models, such as the secondary creep (SC) model, tertiary creep (TC) model, and secondary creep-tertiary creep (SC-TC) combined model. Predicted creep curves obtained by the SC-TC model were significantly more accurate than those corresponding to the cases of the SC model or TC model. The SC-TC model can be applied for predicting the accumulated creep deformation in such cases as the tube expansion or creep cavitation damage.

(3) Microstructure degradation was investigated. The precipitation of $M_{23}C_6$ and G-phase appeared progressively, and coarsening of the precipitate occurred quickly along the grain boundaries during the service period at a high temperature. This could cause the formation of cavities formation resulting in higher creep damage, and consequently promoting the deterioration of the creep resistance.

Acknowledgments

This research was supported by the Chung-Ang University Graduate Research Scholarship (Mr. Jong Min Yu) in 2016. This work was also supported by the KETEP (No. 2013 2010 500060) granted financial resource from the Ministry of Trade, Industry & Energy (MOTIE).

Nomenclature

A	: Creep coefficient of secondary creep stages
A_3	: Creep coefficient of tertiary creep stages
n	: Creep exponent of secondary creep stages
n_3	: Creep exponent of tertiary creep stages
p_3	: Creep constant of tertiary creep stages
σ	: Applied stress
ε	: Total creep strain
ε_{TC}	: Creep strain of tertiary creep stages
$\dot{\varepsilon}$	: Creep strain rate
$\dot{\varepsilon}_{SC}$	: Secondary creep strain rate
$\dot{\varepsilon}_{TC}$	: Tertiary creep strain rate
P	: Larson-Miller parameter
T	: Temperature
t_r	: Creep rupture time
t_t	: Tertiary creep initiation time

References

[1] *API Standard 530, Calculation of Heater-tube Thickness in Petroleum Refineries*, American Petroleum Institute (2015).

[2] E. Guglielmino, R. Pino, C. Servetto and A. Sili, *Handbook of Materials Failure Analysis with Case Studies from the Chemi-*

cals, Concrete and Power Industries, Elsevier Ltd. (2016) 69-91.
[3] N. Roy, A. Raj, B. N. Roy and A. K. Ray, Creep deformation and damage evaluation of service exposed reformer tube, *Canadian Metallurgical Quarterly*, 54 (2) (2015) 205-222.
[4] L. Bonaccorsi, E. Guglielmino, R. Pino, C. Servetto and A. Sili, Damage analysis in Fe-Cr-Ni centrifugally cast alloy tubes for reforming furnaces, *Engineering Failure Analysis*, 36 (2014) 65-74.
[5] A. R. Andrade, C. Bolfarini, L. A. M. Ferreira, A. A. A. Vilar, C. D. Souza Filho and L. H. C. Bonazzi, Influence of niobium addition on the high temperature mechanical properties of a centrifugally cast HP alloy, *Materials Science and Engineering A*, 628 (2015) 176-180.
[6] L. H. de Almeida, A. F. Ribeiro and I. Le May, Microstructural characterization of modified 25Cr-35Ni centrifugally cast steel furnace tubes, *Materials Characterization*, 49 (2002) 219-229.
[7] D. Alessio, G. Gonzalez, V. F. Pirrone, L. Iurman and L. Moro, Variation of creep properties in HP steel by influence of temperature, *Procedia Materials Science*, 1 (2012) 104-109.
[8] G. Pilloni, E. Quadrini and S. Spigarelli, Interpretation of the role of forest dislocations and precipitates in high-temperature creep in a Nb-stabilised austenitic stainless steel, *Materials Science and Engineering A*, 279 (1) (2000) 52-60.
[9] G. D. Barbabela, L. H. de Almeida, T. L. Da Silveira and I. Le May, Role of Nb in modifying the microstructure of heat-resistant cast HP steel, *Materials Characterization*, 26 (1991) 193.
[10] C. J. Liu and Y. Chen, Variations of the microstructure and mechanical properties of HP40Nb hydrogen reformer tube with time at elevated temperature, *Materials and Design*, 32 (4) (2011) 2507-2512.
[11] A. Alvino, D. Ramires, A. Tonti and D. Lega, Influence of chemical composition on microstructure and phase evolution of two HP heat resistant stainless steels after long term plant-service aging, *Material at High Temperature*, 31 (1) (2014) 2-11.
[12] V. H. Dao, J. J. Song, J. Y. Kim and K. B. Yoon, Creep deformation characteristics of microalloyed HP40Nb steel at 950 ^{o}C, *Journal of Mechanical Science and Technology*, 33 (10) (2019) 4813-4821.
[13] J. Swaminathan, K. Guguloth, M. Gunjan, P. Roy and R. Ghosh, Failure analysis and remaining life assessment of service exposed primary reformer heater tubes, *Engineering Failure Analysis*, 15 (2008) 311-331.
[14] A. K. Ray, S. K. Sinha, Y. N. Tiwari, J. Swaminathan, G. Das, S. Chaudhuri and R. Singh, Analysis of failed reformer tubes, *Engineering Failure Analysis*, 10 (3) (2003) 351-362.
[15] R. Voicu, J. Lacaze, E. Andrieu, D. Poquillon and J. Furtado, Creep and tensile behaviour of austenitic Fe-Cr-Ni stainless steels, *Materials Science and Engineering A*, 510 (2009) 185-189.
[16] A. Ghatak and P. S. Robi, A comparative study of constitutive equations for the creep deformation of HP40Nb micro-alloyed steel, *Materials Science and Engineering A*, 648 (2015) 418-427.
[17] A. Ghatak and P. S. Robi, High-temperature deformation behavior of HP40Nb micro-alloyed reformer steel, *Metallography, Microstructure and Analysis*, 4 (6) (2015) 508.
[18] B. F. Dyson and T. B. Gibbons, Tertiary creep in nickel-base superalloys: Analysis of experimental data and theoretical synthesis, *Acta Metallurgica*, 35 (9) (1987) 2355-2369.
[19] C. M. Stewart, A. P. Gordon, Y. W. Ma and R. W. Neu, An anisotropic tertiary creep damage constitutive model for anisotropic materials, *International Journal of Pressure Vessels and Piping*, 88 (8-9) (2011) 356-364.
[20] C. M. Stewart, E. A. Hogan and A. P. Gordon, Modeling the temperature-dependence of tertiary creep damage of a directionally solidified Ni-base superalloy, *ASME 2009 International Mechanical Engineering Congress and Exposition*, American Society of Mechanical Engineers Digital Collection, January (2009) 17-25.
[21] *ASTM E-139-11*, *Standard Test Method for Conducting Creep, Creep-rupture, and Stress-rupture Test of Metallic Materials,* ASTM International (1994).
[22] *ASTM E-647-15*, *Standard Test Method for Measurement of Fatigue Crack Growth Rates*, ASTM International (2004).
[23] V. H. Dao, K. B. Yoon, G. M. Yang and J. S. Oh, Determination of creep constitutive model for 28-48 WCo alloy based on experimental creep tests at 817-982 °C, *J. of Mechanical Science and Technology*, 32 (9) (2018) 4201-4208.
[24] A. R. Andrade, C. Bolfarini, L. A. M. Ferreira, C. D. Souza Filho and L. H. C. Bonazzi, Titanium micro addition in a centrifugally cast HPNb alloy: High temperature mechanical properties, *Materials Science and Engineering: A*, 636 (2015) 48-52.
[25] S. Latha, M. D. Mathew, P. Parameswaran, K. B. S. Rao and S. L. Mannan, Thermal creep properties of alloy D9 stainless steel and 316 stainless steel fuel clad tubes, *Int. of Pressure Vessels and Piping*, 85 (2008) 866-870.
[26] J. T. Staley Jr. and A. Saxena, Mechanisms of creep crack growth in 1 wt% antimony-copper: Implications for fracture parameters, *Acta Metallurgica et Materialia*, 38 (6) (1990) 897-908.
[27] G. D. A. Soares, L. H. Almeida, T. L. Silveira and I. Le May, Niobium additions in HP heat-resistant cast stainless steels, *Material Characterization*, 29 (1992) 387-396.
[28] M. Hillert, The compound energy formalism, *Journal of Alloys and Compounds*, 320 (2) (2001) 161-176.
[29] M. Abbasi, I. Park, Y. Ro, Y. Ji, R. Ayer and J. H. Shim, G-phase formation in twenty-years aged heat-resistant cast austenitic steel reformer tube, *Materials Characterization*, 148 (2019) 297-306.
[30] C. Phaniraj, M. Nandagopal, S. L. Mannan, P. Rodriguez and B. P. Kashyap, Analysis of first order kinetics for tertiary creep in AISI 304 stainless steel, *Acta Materialia*, 44 (10) (1996) 4059-4069.

Jong Min Yu received his M.S. in Mechanical Engineering from Chung-Ang University. He is currently a Ph.D. candidate in Chung-Ang University. His research interest is life and integrity assessment of facilities in power and process plants. He is also interested in creep fracture of additive manufactured components.

Van Hung Dao received his M.S. and Ph.D. degrees in Mechanical Engineering from Chung-Ang University. He is currently a postdoctoral fellow at Chung-Ang University. His research interests are microstructural analysis and application of high temperature fracture mechanics to life assessment of structural material. He is extending research to behavior of additive manufactured materials.

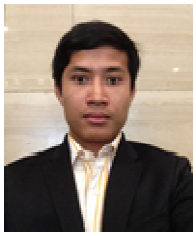

Vanno Lok received his B.S. in Industrial and Mechanical Engineering from Institute of Technology of Cambodia. He received M.S. in Mechanical Engineering from Chung-Ang University. He is currently a Ph.D. candidate in Chung-Ang University. His research interests are stress analysis problem in pressure vessel & piping application in power plant and microstructural analysis of high temperature fracture mechanics to structural materials in life assessment.

Thi Giang Le received her B.S. in Metallurgical Engineering from Hanoi University of Science and Technology. She received M.S. and Ph.D. in mechanical engineering from Chung-Ang University. Her research interest is creep behavior and aging characteristics of the high temperature alloy materials.

Kee Bong Yoon received his B.S. in Mechanical Engineering from Seoul National University, M.S. from KAIST and Ph.D. from Georgia Institute of Technology. He is currently a Professor at Chung-Ang University. His research interests are high temperature fracture and risk based management of energy plants and semiconductor plants. He is extending research to fracture of additive manufactured materials.